

Thermal Topology Collapse: Universal Physical Patch Attacks on Infrared Vision Systems

Chengyin Hu¹, Yikun Guo¹, Yuxian Dong¹, Qike Zhang¹, Kalibinuer Tiliwalidi², Yiwei Wei³, Haitao Shi⁴, Jiujiang Guo³, Jiahuan Long^{5*}, and Xiang Chen¹

¹ China University of Petroleum-Beijing at Karamay, NO. 355, Anding Road, Karamay, 834000, Xinjiang, China

² University of Electronic Science and Technology of China, No. 2006, Xiyuan Avenue, Gaoxin District, Chengdu, 611731, Sichuan, China

³ College of Intelligence and Computing, Tianjin University

⁴ School of software, Shandong University

⁵ Shanghai Jiaotong University

Abstract. Although infrared pedestrian detectors have been widely deployed in visual perception tasks, their vulnerability to physical adversarial attacks is becoming increasingly apparent. Existing physical attack methods predominantly rely on instance-specific online optimization and rigid pattern design, leading to high deployment costs and insufficient physical robustness. To address these limitations, this work proposes the Universal Physical Patch Attack (UPPA), the first universal physical attack method in the infrared domain. This method employs geometrically constrained parameterized Bézier blocks to model perturbations and utilizes the Particle Swarm Optimization (PSO) algorithm to perform unified optimization across the global data distribution, thus maintaining topological stability under dynamic deformations. In the physical deployment phase, we materialize the optimized digital perturbations into physical cold patches, achieving a continuous and smooth low-temperature distribution that naturally aligns with the thermal radiation characteristics of infrared imaging. Extensive experiments demonstrate that UPPA achieves an outstanding physical attack success rate without any online computational overhead, while also exhibiting strong cross-domain generalization and reliable black-box transferability.

Keywords: Infrared pedestrian detectors · Universal physical patch attack · Bézier blocks

1 Introduction

Recently, Deep Neural Networks (DNNs) have achieved transformative breakthroughs in image classification [13] and object detection [32]. However, visible-light signals are susceptible to severe degradation in uncontrolled environments [34], making infrared thermal imaging a critical alternative for

* Corresponding author

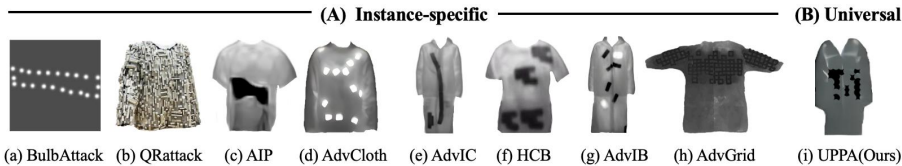


Fig. 1: Infrared physical attack methods against pedestrian detectors. (A) Instance-specific methods [14, 15, 40–42, 46–48]; (B) Universal (UPPA, ours).

all-weather, highly reliable perception systems [18]. Despite their environmental adaptability, infrared detectors inherit the vulnerability of DNNs to adversarial examples [22, 49].

Existing infrared physical attacks (as illustrated in Fig. 1) have evolved from early active heat sources [47, 48] toward passive, stealthy designs [14, 15, 40, 41]. While the theoretical feasibility of universal adversarial perturbations has been extensively validated in the visible domain [37], the physical constraints of thermal diffusion and low spatial resolution in the infrared spectrum prevent the formation of high-frequency discrete textures, restricting most methods [14, 40, 41] to simple rigid geometric blocks. To ensure attack efficacy, these approaches are forced to perform highly customized optimization for specific pedestrian poses and spatial scales, resulting in a fundamental instance-specific bottleneck. This “single-sample-single-optimization” mechanism suffers from two fatal limitations: (1) extreme online computational latency that precludes real-time deployment, and (2) a lack of physical robustness, where perturbations overfit to static frames and fail instantaneously during real-world dynamic pose changes.

To break these limitations and fill the gap in universal physical attacks within the infrared domain, we propose the first Universal Physical Patch Attack (UPPA) against infrared pedestrian detectors, aiming to capture the modal commonalities of vulnerabilities in infrared data distributions. Addressing the inability of infrared media to represent high-frequency pixels, we innovatively introduce parameterized Bézier curves for the geometric modeling of perturbation morphology, ensuring physical smoothness while compressing high-dimensional pixel space into a compact parameter space. Subsequently, we combine the Particle Swarm Optimization (PSO) algorithm [20] for efficient global optimization, deeply integrating Thin Plate Spline (TPS) [2] and Expectation over Transformation (EOT) [1] to explicitly model non-rigid deformations and complex physical transformations, thereby effectively bridging the cross-domain gap between digital and physical environments. By extracting instance-agnostic adversarial features offline, the universal perturbations generated by UPPA can be directly deployed, completely eliminating online computational overhead during the operational phase. In summary, our key contributions include:

- **Universal attack method.** We propose the first universal physical patch attack method against infrared pedestrian object detectors. Through unified optimization over the global data distribution, UPPA applies a single

shared perturbation across all instances, overcoming the instance-specific limitations of existing approaches and significantly enhancing attack scalability in dynamic environments.

- **Physical efficacy and transferability.** Systematic evaluations demonstrate that UPPA maintains high stability across diverse digital scenarios, including extreme weather conditions and black-box transfer settings, while achieving exceptional attack success rates in real-world environments.
- **Mechanistic insight and efficiency.** Grad-CAM-based analyses reveal that parameterized Bézier structures profoundly suppress semantic features. UPPA resists image-restoration defenses and achieves zero online computational overhead through an entirely offline universal generation mechanism.

2 Related Works

2.1 Physical Attacks in the Visible Domain

In the visible field, physical adversarial attacks aim to expose the security vulnerabilities of deep learning models in complex real-world environments [5]. Thys et al. [39] pioneered the evasion of person detectors through local physical patches. Subsequently, the research focus shifted toward enhancing attack robustness and stealthiness. For non-rigid targets, researchers introduced Thin-Plate Spline (TPS) [2] and flexible transformation techniques to simulate clothing wrinkles, ensuring attack effectiveness under dynamic deformation [17, 43], while more recent works further explore dynamic, naturalistic adversarial patches for person detectors [9]. For rigid targets (e.g., vehicles), related studies utilized neural approximation functions and full-coverage textures to achieve highly robust camouflage [23, 27, 28, 45]. Additionally, to reduce the risk of human visual perception, natural lighting simulation and Generative Adversarial Networks (GANs) were used to generate camouflage patterns possessing both stealthiness and aggressiveness [16, 36]. However, the aforementioned methods highly depend on high-frequency textures and fine color combinations in the RGB space. Since the infrared imaging mechanism depends entirely on the target’s thermal radiation distribution, this visible-light attack paradigm, which relies on spatial spectral features, is difficult to achieve effective physical reconstruction in the thermal imaging modality.

2.2 Physical Attacks in the Infrared Domain

Considering the particularity of the infrared modality, existing research has evolved from active interference to passive perturbation (Fig. 1). Early methods such as Bulbs Attack [48] and AdvCloth [47] rely on light bulbs or heating films to generate active hot spots, but their dependence on external power sources limits their stealthiness and long-term deployment in real-world scenarios. Consequently, research has shifted toward passive attacks based on cold and hot media. QRattack [46] and AIP [42] utilize thermal insulation materials to

construct pixelated patterns under a white-box setting. To address robustness challenges in black-box scenarios, HCB [41] pioneers the use of hot-cold patch mechanisms. Subsequent works such as AdvIB [14], AdvIC [15], and AdvGrid [40] achieve more refined physical attack effects through discrete block modeling, parameterized Bézier curves, and evolutionary optimization, respectively. Despite significant progress, the instance-specific nature of these methods severely limits their practicality. When faced with changes in scenes or poses, attackers must re-execute expensive iterative optimizations or even remanufacture and redeploy physical media. This high computational overhead and physical reconstruction cost result in a lack of scalability and practical potential in dynamic real-time scenarios.

2.3 Universal Adversarial Attacks

Universal adversarial perturbations decouple optimization from specific samples, with proven efficacy in digital [21, 31], physical [26], and black-box [37] domains. However, existing mechanisms rely heavily on rich colors and high-frequency textures. Due to the absence of color and the low-frequency constraints of thermal diffusion, migrating these visible-light paradigms to infrared imaging encounters a severe physical gap. Consequently, a universal infrared attack paradigm satisfying both physical smoothness and common modal features remains lacking.

Existing infrared physical attacks incur high computational costs due to instance-specific optimization, while visible-light universal attacks struggle to transfer across the physical characteristics of thermal radiation. To address this gap, we introduce UPPA, a universal attack method based on parameterized Bézier blocks that enables robust physical adversarial evasion without online computation.

3 Methods

This section introduces UPPA, a universal physical patch attack that consistently fools infrared pedestrian detectors across identities and scenarios. As shown in Fig. 2, it comprises: (1) digital optimization of topologically constrained Curved-Blocks via global black-box parameter tuning; (2) robustness modeling via EOT [1] and TPS [2]; and (3) physical deployment as wearable cold patches.

3.1 Problem Definition

Let the infrared pedestrian dataset be denoted as $\mathcal{J} = \{X, Y\}$, where $X \in \mathbb{R}^{H \times W}$ is a clean infrared image and Y is the corresponding ground-truth label. Given a pre-trained pedestrian detector $f: X \rightarrow Y$, its prediction on an input X can be written as

$$y = (y_{\text{pos}}, y_{\text{obj}}, y_{\text{cls}}) = f(X), \quad (1)$$

where y_{pos} denotes bounding-box coordinates, y_{obj} the objectness scores, and y_{cls} the class probabilities.

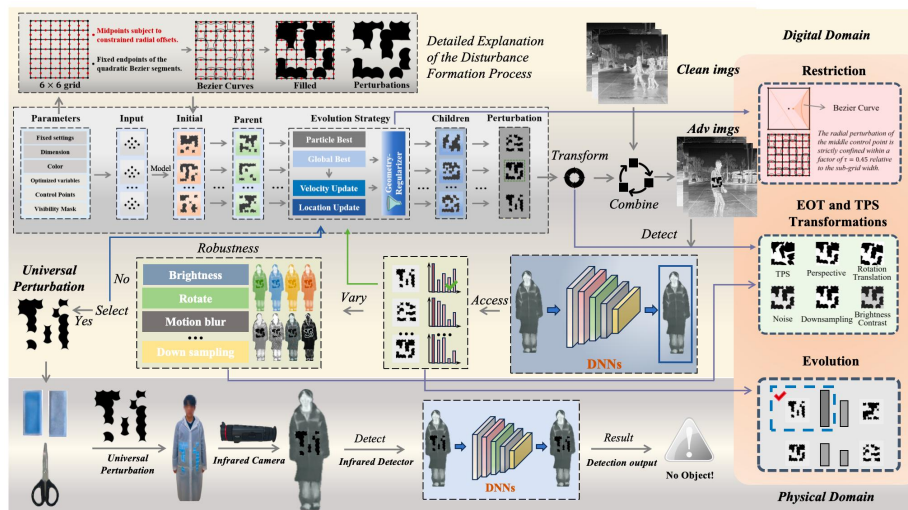


Fig. 2: Overall framework of UPPA.

Unlike instance-specific physical attacks that optimize a dedicated perturbation for each sample, UPPA seeks an optimal universal parameter configuration θ^* that generalizes across the entire data distribution. We define the adversarial sample set generated under parameters θ as

$$\mathcal{J}_{\text{adv}}(\theta) = \left\{ X_{\text{adv}}^{(i)} = S(X^{(i)}, \theta, M^{(i)}) \mid (X^{(i)}, Y^{(i)}) \in \mathcal{J} \right\}, \quad (2)$$

where $\theta = (D, W, \delta, C)$ comprehensively establishes the physical attributes of the Curved-Blocks: D and W control perturbation dimensions and width, δ specifically modulates the curvature of the edges within the curved-block units, and $C \in \{0, 1\}^{D \times D}$ serves as a visibility mask to precisely control the activation and deactivation of thermal radiation. The spatial mask $M^{(i)}$ constrains the perturbation to the pedestrian region in $X^{(i)}$, and $S(\cdot)$ denotes the linear fusion of the clean sample and the simulated infrared Curved-Blocks.

To bridge the gap between digital simulations and the physical world, we introduce a stochastic physical transformation distribution \mathcal{T} . Each transformation $\Gamma \sim \mathcal{T}$ composes environmental variations modeled by EOT [1] (e.g., scaling, translation, sensor noise) with non-rigid clothing deformations modeled by TPS [2]. The universal attack objective is then formulated as minimizing the expected detection confidence over all adversarial samples and random physical transformations:

$$\theta^* = \arg \min_{\theta \in \Omega} \mathbb{E}_{(X, Y) \in \mathcal{J}_{\text{adv}}(\theta), \Gamma \sim \mathcal{T}} [y_{\text{obj}} \leftarrow f(\Gamma(X))], \quad (3)$$

where Ω denotes the feasible parameter space that satisfies the geometric constraints of the Bézier-based Curved-Blocks.

3.2 Parametric Modeling of Topologically Constrained Curved-Blocks

UPPA models the perturbation as structured Bézier Curved-Blocks composed of $D \times D$ sub-units. This parametric design greatly compresses the optimization space while guaranteeing geometric continuity and manufacturability.

Block Parameterization and Axial Locking. Each edge of a solid Curved-Block unit is represented by a quadratic Bézier curve $B(t)$ controlled by three points $\{P_0, P_1, P_2\}$:

$$B(t) = (1-t)^2P_0 + 2t(1-t)P_1 + t^2P_2, \quad t \in [0, 1]. \quad (4)$$

Here P_0 and P_2 are fixed endpoints anchored at the vertices of an initial regular grid, while P_1 is a curvature control point. To reduce fabrication complexity and improve robustness, we adopt an axial locking mechanism: P_1 is allowed to move only along the normal direction of the corresponding grid edge,

$$P_1 = P_1^{(0)} + \delta n, \quad n \in \{e_x, e_y\}, \quad (5)$$

where $P_1^{(0)}$ is the midpoint of the edge in the regular grid, δ is the deformation parameter to be optimized, and n is determined by the edge direction: for a horizontal edge, n is locked to $e_y = [0, 1]^\top$; for a vertical edge, n is locked to $e_x = [1, 0]^\top$. This one-dimensional control preserves topological consistency while still granting sufficient geometric flexibility.

Convex-Hull Constraint and Topological Integrity. Unconstrained updates of δ often lead to adjacent Curved-Blocks overlapping topologies and structural collapse (Fig. 3 (a)), generating “parameter dead zones” that hinder convergence efficiency. To eliminate such geometric collisions, UPPA leverages the convex-hull property of Bézier curves [6], which ensures that each curve segment resides within the triangle formed by its control points. We further partition each solid Curved-Block unit into four non-overlapping triangular territories along the diagonals, as illustrated in Fig. 3 (c), and restrict the one-dimensional orthogonal offset of the intermediate control point P_1 to remain within its designated territory. This design preserves topological integrity while maximizing the deformation space, yielding a globally stable Curved-Blocks configuration (Fig. 3 (b)). Based on this construction, we derive a radial safety threshold for the deformation parameter δ :

$$|\delta| \leq \tau d, \quad (6)$$

where d denotes the spacing of the regular grid. Considering the theoretical tangency limit of $0.5d$ (Fig. 3 (d)), beyond which adjacent curves collide and topology breaks down (Fig. 3 (e)), we adopt a conservative setting of $\tau = 0.45$ (Fig. 3 (c)), which grants the perturbation sufficient geometric expressiveness while maintaining a robust safety margin under extreme physical deformations.

3.3 Black-Box Optimization via Particle Swarm Optimization

During physical deployment, infrared pedestrian detectors are typically accessed in a black-box manner and do not expose internal gradients. UPPA therefore

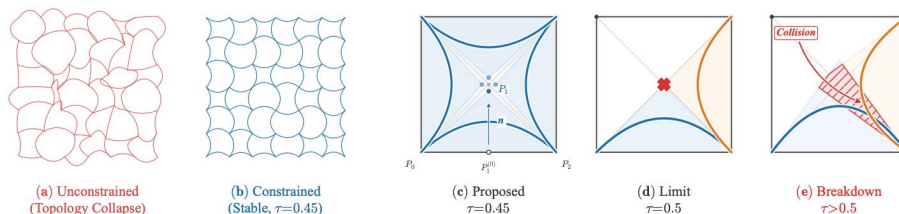


Fig. 3: Topology-constrained optimization of Curved-Blocks.

reformulates the objective as a fitness maximization problem and solves it using Particle Swarm Optimization (PSO) [20].

For a given parameter configuration θ , we define the universal fitness function $F(\theta)$ by the average confidence \bar{y}_{obj} over the adversarial sample set $\mathcal{J}_{\text{adv}}(\theta)$:

$$F(\theta) = 1 - \bar{y}_{\text{obj}} = 1 - \frac{1}{|\mathcal{J}_{\text{adv}}(\theta)|} \sum_{X_{\text{adv}}^{(i)} \in \mathcal{J}_{\text{adv}}(\theta)} \mathbb{E}_{\Gamma \sim \mathcal{T}} [y_{\text{obj}} \leftarrow f(\Gamma(X_{\text{adv}}^{(i)}))]. \quad (7)$$

Intuitively, a lower confidence corresponds to a higher attack success rate, so maximizing $F(\theta)$ is equivalent to minimizing the detector’s reliability.

Distinct from instance-specific attacks, UPPA jointly optimizes θ over the whole digital sample set, driving particles to discover structural vulnerabilities that are shared across different pedestrians, scenes, and detectors. After each update, a topological validity check is performed: if any deformation parameter violates the safety bound $|\delta| > \tau d$, it is projected back to the feasible region Ω via

$$\delta \leftarrow \text{sgn}(\delta) \cdot \min(|\delta|, \tau d), \quad (8)$$

thereby eliminating invalid configurations and focusing the swarm optimization on high-quality feasible regions. This strategy significantly improves convergence stability and yields universal Curved-Blocks with strong attack performance in both digital and physical domains.

4 Experiments

4.1 Experimental Setting

Datasets. We employ the FLIR v1_3 [7] dataset as the training and primary evaluation benchmark, strictly filtering out pedestrian instances shorter than 120 pixels to ensure sample quality. To comprehensively verify the generalization performance of the attack in dynamic real-world scenarios, we introduce four additional datasets with specific physical challenges: FLIR v2 [38] for cross-sensor imaging, LLVIP [19] focusing on low-light night scenes, MFNet [10] with complex scenes and significant scale variations, and M3FD [25] encompassing diverse weather conditions.

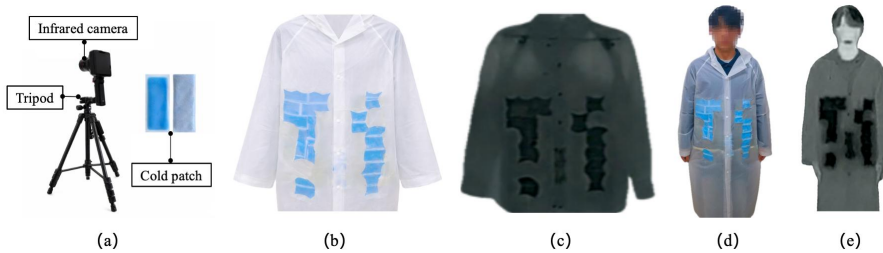


Fig. 4: Experimental devices and physical deployment. (a) Infrared camera, tripod, and cold patch. (b) Visible spectrum image of the clothing. (c) Infrared image of the clothing. (d) Visible spectrum image of a pedestrian. (e) Infrared image of a pedestrian.

Object Detectors. To ensure a comprehensive evaluation, we selected nine advanced detectors covering mainstream architectures: two-stage networks (Faster R-CNN [33], Mask R-CNN [12], Libra R-CNN [30]), one-stage networks (YOLOv3 [32], RetinaNet [24], YOLOF [4], YOLOX [8]), and Transformer-based models (DETR [3], Deformable-DETR [50]). These models achieve mean Average Precision ranging from 88.0% to 93.0% on the clean FLIR v1_3 test set, forming an exceptionally robust defense baseline. In all attack experiments, YOLOv3 is used by default as the proxy model to generate universal perturbations.

Experimental Devices. The setup (Fig. 4(a)) includes an infrared camera, a tripod, and physical cold patches. For visualization, the patches are placed inside a transparent raincoat according to the optimized Bézier layout (Fig. 4(b)); in practice, they can be hidden under opaque clothing for complete visible-spectrum stealth. In infrared images, the perturbations appear as smooth-bounded, low-temperature dark regions (Fig. 4(c)). In the on-body demo (Fig. 4(d,e)), the patches are only visible due to the transparent coat, while remaining effective yet fully concealed under regular clothing.

Baselines and Metrics. We evaluate HCB [41], AdvIC [15], and AdvGrid [40] as representative infrared black-box baselines. Originally instance-specific, we adapt them to a universal setting by optimizing a shared patch over the training set. Unlike online per-sample attacks, UPPA follows an offline universal optimization paradigm where query counts are fixed by preset hyperparameters— independent of sample difficulty. Thus, query count is not a real-time efficiency metric. Attack Success Rate (ASR) is the primary metric, defined as the ratio of correctly detected targets whose confidence drops below 0.5 after perturbation:

$$\text{ASR} = 1 - \frac{1}{N_t} \sum_{n_1=1}^{N_t} \mathbb{I}(y_{\text{obj}}^{n_1}), \quad \mathbb{I}(y_{\text{obj}}^{n_1}) = \begin{cases} 0, & y_{\text{obj}}^{n_1} < 0.5 \\ 1, & \text{otherwise} \end{cases} \quad (9)$$

where N_t denotes the true positive targets detected without attacks, $y_{\text{obj}}^{n_1}$ is the predicted confidence of the n_1 -th target under attack, and the detection threshold is 0.5.

Table 1: Experimental results of deploying UPPA across different detectors and datasets (%).

	FLIR v1_3 [7]	FLIR v2 [38]	LLVIP [19]	MFNet [10]	M3FD [25]
Faster R-CNN	89.91	82.79	81.72	96.00	74.83
YOLOF	86.45	77.49	76.19	97.10	65.50
Mask R-CNN	85.05	75.43	74.05	91.86	68.04
Libra R-CNN	75.00	61.82	60.08	95.54	50.03
YOLOv3	62.42	47.27	45.45	86.21	35.66
RetinaNet	44.30	30.03	26.76	74.96	19.55
YOLOX	42.14	28.22	28.52	73.27	20.97
Deformable-DETR	23.24	12.02	13.18	53.26	9.18
DETR	20.20	14.05	11.27	48.79	7.79
Average ASR (%)	58.75	47.68	46.36	79.67	39.06

Implementation Details. The dimension of the adversarial Curved-Blocks is set to $D = 6$, with the width restricted to $1/4$ of the target bounding box height. The topological safety threshold is set to $\tau = 0.45$. The hyperparameters of the PSO algorithm [20] used for global optimization are configured as follows: population size $N = 50$, maximum iterations $K = 10$, inertia weight $\omega = 0.9$, cognitive and social coefficients $c_1 = 1.6$ and $c_2 = 1.4$, respectively, and random factors $r_1 = 0.5$ and $r_2 = 0.5$. This configuration achieves an optimal balance between computational overhead and convergence stability. All experiments are conducted on a single NVIDIA RTX 4090 GPU.

4.2 Effectiveness Evaluation

Digital Attacks. We deploy UPPA and evaluate it on nine detectors across five thermal datasets (See Table 1). Overall, the attack achieves consistently high ASR on CNN-based detectors and remains stable across domains. Performance is strongest on MFNet (average ASR 79.67%), while FLIR v1_3/v2 and LLVIP show stable effectiveness (58.75%/47.68%/46.36%). M3FD is the most challenging benchmark (39.06%), indicating a larger domain shift that weakens attack performance. Across models, two-stage and CNN-style detectors are more vulnerable: Faster R-CNN, Mask R-CNN, and YOLOF reach very high ASR, peaking around 96%–97% on MFNet and staying competitive on other datasets. In contrast, Transformer-based detectors (DETR and Deformable-DETR) are notably more robust, with much lower ASR, especially on M3FD. Fig. 5 visualizes the adversarial samples generated by UPPA, showing that the learned universal perturbation can effectively carry out adversarial attacks.

Physical Attacks. To evaluate the adversarial efficacy of UPPA in the physical domain, we conduct physical experiments specifically targeting YOLOv3 [32]



Fig. 5: Digital samples generated by UPPA.

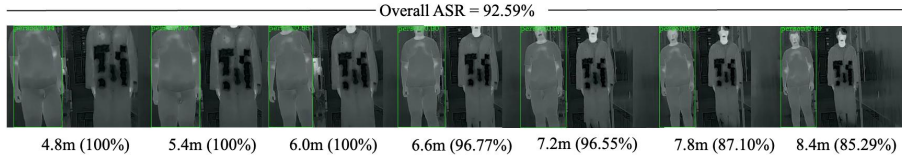


Fig. 6: Physical samples and experimental results of UPPA.

across distances from 4.8 m to 8.4 m. UPPA demonstrates formidable potency at near ranges (4.8 m–6.0 m), achieving a 100% ASR. Even under the stringent conditions of 8.4 m, where infrared sensor resolution significantly degrades, the ASR remains as high as 85.29%. With an overall ASR of 92.59%, these results conclusively demonstrate the effectiveness of UPPA in the physical domain. Typical physical samples and the corresponding experimental results are shown in Fig. 6, with video demonstrations provided in the Supplementary Material.

4.3 Stealthiness Evaluation

We evaluate the stealthiness of UPPA through both subjective ratings and an objective metric; in a subjective study, twenty volunteers rated physical sample images on a 5-point scale, yielding mean scores of 2.65, 3.20, 2.55, and 3.60 for HCB [41], AdvIC [15], AdvGrid [40], and UPPA, respectively. UPPA’s smooth Bézier boundaries better mimic natural clothing folds, whereas rigid blocks and grid textures are perceived as conspicuous artifacts. We further quantify stealthiness by computing the LPIPS metric [44] within the local patch region localized by pixel differences: UPPA achieves the best score (0.3667), outperforming HCB (0.3864), AdvIC (0.3724), and AdvGrid (0.4776), which confirms that the smoothness of Bézier curves aligns the generated patterns more closely with real-world infrared thermodynamic distributions.

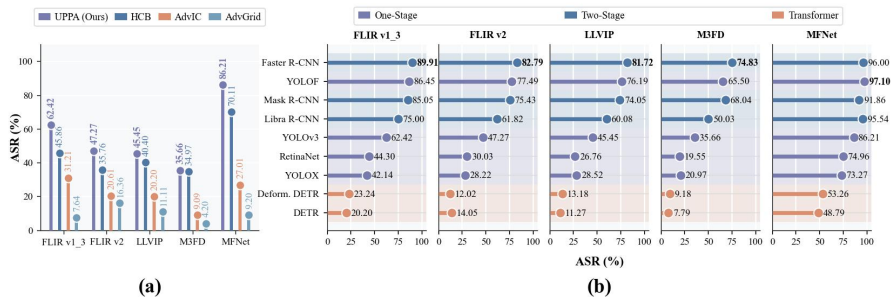


Fig. 7: (a) Comparison with Baseline Methods; (b) Cross-Dataset Transfer.

4.4 Comparison with Baseline Methods

We compare UPPA with representative infrared black-box baselines HCB [41], AdvIC [15], and AdvGrid [40] across the five datasets. As shown in Fig. 7 (a), UPPA consistently outperforms existing methods on all benchmarks. On MFNet [10], which features complex backgrounds and rich thermal textures, UPPA attains an ASR of 86.21%, yielding an absolute improvement of 16.1 percentage points over the second-best baseline (HCB at 70.11%). Even under the challenging conditions of M3FD [25], UPPA still maintains the highest performance. These results demonstrate that topology-constrained Curved-Blocks provide stronger and more stable attack performance than existing discrete-block or grid-based designs.

5 Discussion

5.1 Transferability Evaluation

Cross-Dataset Transfer. We evaluate cross-dataset universality by optimizing a single universal perturbation on FLIR v1_3 for each detector and then directly deploying the same perturbation to four unseen datasets (FLIR v2, LLVIP, MFNet, and M3FD) **without any fine-tuning** (See Fig. 7 (b)). Overall, UPPA exhibits strong transferability across domains for most detectors. In particular, the attack remains highly effective on MFNet, where the ASR is consistently high (e.g., YOLOv3: 77.01%, YOLOF: 86.29%, Mask R-CNN: 85.15%, Faster R-CNN: 90.43%), and in several cases even matches or exceeds the source-dataset performance (e.g., YOLOv3 improves from 62.42% on FLIR v1_3 to 77.01% on MFNet). Transfer to FLIR v2 and LLVIP remains competitive for most CNN-based models (typically around the 30% to 70% range depending on the backbone), demonstrating that the learned perturbation is not merely overfitting to FLIR v1_3-specific statistics. By contrast, M3FD is generally the most challenging target, where ASR drops across detectors (e.g., YOLOX: 20.24%, DETR:

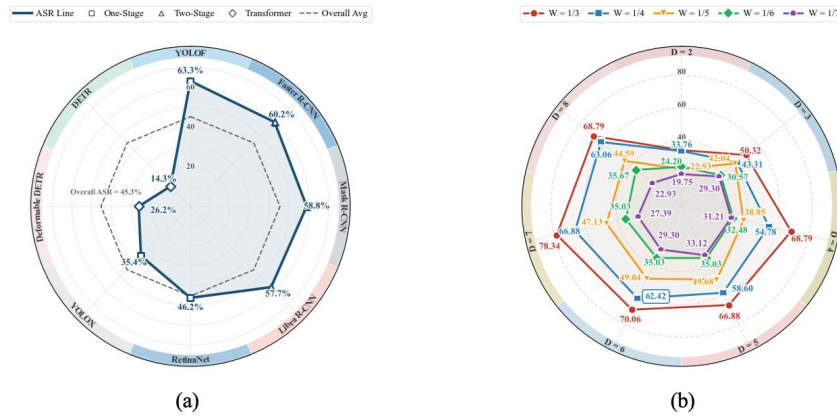


Fig. 8: (a) Cross-model transfer; (b) Ablation of dimension-width.

13.59%, Deformable-DETR: 18.67%), suggesting a larger domain shift in acquisition conditions and thermal appearance.

Cross-Model Transfer. To assess black-box cross-model transfer, we craft adversarial samples on YOLOv3 [32] and evaluate them on other detectors. Fig. 8(a) shows strong transfer to CNN-based models (ASR 63.3% on YOLOF [4], 60.2% on Faster R-CNN [33]), suggesting our Bézier Curved-Blocks effectively disrupt convolutional spatial priors. Transfer is weaker on Transformer-based detectors (26.2% on Deformable-DETR [50], 14.3% on DETR [3]), consistent with the robustness of global self-attention. Overall, the high transferability across widely used CNN detectors highlights a practical security risk for infrared surveillance.

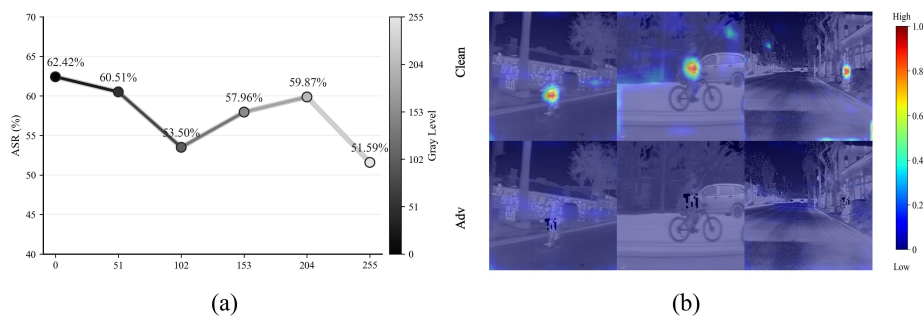
5.2 Ablation Study

Ablation of dimension and width. We next evaluate the interplay between the Curved-Block dimension D and relative width W to optimize the trade-off between attack efficacy and visual stealth. As illustrated in Fig. 8 (b), the ASR positively correlates with W , as wider perturbations more effectively override the target’s intrinsic thermal signature to induce detection failure. Regarding the dimension D , performance peaks at $D = 7$ but slightly declines at $D = 8$ due to structural over-fragmentation. While the configuration $D = 7$, $W = 1/3$ achieves a maximum ASR of 78.34%, it compromises visual naturalness by generating excessive solid regions. Consequently, we select $D = 6$, $W = 1/4$ as the default configuration, achieving a robust 62.42% ASR while ensuring that the perturbation blends naturally into clothing contours.

Effectiveness of the Bézier boundary deformation mechanism. To justify the necessity of Bézier-based boundary parameterization, we conduct an ablation study comparing UPPA with three alternatives: Straight Blocks, Polyline Blocks, and Catmull-Rom Blocks. As presented in Table 2, the rigid baselines achieve 52.23% and 55.57% ASR respectively, while the flexible Catmull-Rom

Table 2: Ablation on boundary geometry.

Method	Boundary Geometry	ASR (%)
Straight Blocks	Rigid straight-edged	52.23
Polyline Blocks	Rigid straight-edged (segment endpoints)	55.57
Catmull-Rom Blocks	Flexible Catmull-Rom spline	57.21
UPPA (Ours)	Flexible Bézier-curved	62.42

**Fig. 9:** (a) Ablation of grayscale level for Curved-Blocks; (b) Grad-CAM visualization of the detector under clean and adversarial samples.

spline reaches 57.21%. UPPA with Bézier-curved boundaries attains the highest ASR of 62.42%. This progression indicates that rigid geometric patterns fail to disrupt the complex, non-rigid semantic structures characteristic of human targets; among flexible parameterizations, the Bézier formulation exhibits superior geometric adaptability, aligning with human contours and clothing folds to achieve a more profound suppression of deep feature activations within the detection network.

Ablation of color. In infrared physical attacks, both the image and the perturbation are represented in grayscale. To investigate the effects of different grayscale values on UPPA’s adversarial effectiveness, we adjust the perturbation to various grayscale levels from black (0, 0, 0) to white (255, 255, 255). As illustrated in Fig. 9 (a), the black perturbation achieves a peak ASR of 62.42%, significantly outperforming the white perturbation (51.59%). Overall, the ASR exhibits a downward trend as the grayscale value increases. This performance gap arises because the high thermal contrast between a black perturbation and a warm pedestrian effectively disrupts the target’s continuous thermal gradients and semantic features, whereas a white perturbation easily blends into the inherent bright thermal signals. Therefore, black is chosen as the default configuration to simulate the maximized adversarial interference of physical low-temperature media (e.g., cold patches).

Table 3: Evaluation of adversarial defenses against UPPA on YOLOv3.

	No defense	AT-1	AT-2	DW
ASR (%)	62.42	1.27	3.80	54.14

5.3 Visual Analysis of Attack Mechanism

To investigate the attack mechanism of UPPA, we visualize the deep feature responses of the YOLOv3 backbone using Grad-CAM [35]. As illustrated in Fig. 9 (b), a qualitative analysis is performed on a representative sample under a fixed normalization scale to ensure the absolute comparability of feature intensities. In the clean image (top row), activation is highly concentrated on the pedestrian’s torso and core regions, reflecting effective feature aggregation for target representation. Conversely, applying the UPPA perturbation (bottom row) causes a drastic collapse in the aggregation pattern. Rather than shifting to the background, the intense activation undergoes global attenuation into a uniform, low-intensity distribution.

5.4 Adversarial Defenses

To assess UPPA under practical defenses, we evaluate its performance on YOLOv3 against two widely used mechanisms: adversarial training [29] and digital watermarking with non-blind inpainting [11]. Results are summarized in Table 3.

Adversarial Training (AT). We conduct two experiments under this defense. In the first setting (AT-1), we directly apply the attack using the optimal patch obtained in Section 4.2. In the second (AT-2), we rerun UPPA under adversarial training to re-optimize and generate a new universal perturbation for attack. The results indicate that adversarial training provides strong protection in both cases: it almost completely neutralizes the known perturbation, reducing ASR to 1.27%, and remains highly effective against the re-optimized, previously unseen perturbation, limiting ASR to 3.80%. This suggests that adversarial training substantially improves robustness to UPPA-style structured physical perturbations, although a small residual vulnerability persists. **Digital Watermarking (DW).** In contrast, digital watermarking with non-blind inpainting remains largely ineffective: UPPA still achieves a 54.14% ASR. This is likely because the smooth, low-frequency Bézier blocks are strongly coupled with the target’s semantic content, making them difficult to remove without degrading pedestrian features. As a result, inpainting-based defenses struggle to eliminate the perturbation while preserving detection-relevant cues.

6 Conclusion

This work proposes UPPA, the first universal physical patch attack method for infrared pedestrian detection. By coupling physically constrained Bézier topologies

with robustness enhancement strategies, the method generates instance-agnostic Curved-Blocks that jointly ensure high physical realizability and spatial continuity. Extensive evaluations demonstrate that UPPA exhibits exceptional cross-domain generalization and black-box transferability across various mainstream detectors. Furthermore, its smooth topological characteristics endow it with inherent resistance against typical image inpainting defenses. In summary, this work reveals deep-seated vulnerabilities of current infrared perception systems in extracting modality-common features, and establishes a forward-looking security evaluation benchmark and theoretical foundation for extending such universal physical attacks to complex multimodal perception systems, such as emerging infrared Vision-Language Models.

References

1. Athalye, A., Engstrom, L., Ilyas, A., Kwok, K.: Synthesizing robust adversarial examples. In: International conference on machine learning. pp. 284–293. PMLR (2018)
2. BOOKSTEIN, F.L.: Principal warps: Thin-plate splines and the decomposition of deformations. *IEEE TRANSACTIONS ON PATTERN ANALYSIS AND MACHINE INTELLIGENCE* **11**, 567 (1989)
3. Carion, N., Massa, F., Synnaeve, G., Usunier, N., Kirillov, A., Zagoruyko, S.: End-to-end object detection with transformers. In: European conference on computer vision. pp. 213–229. Springer (2020)
4. Chen, Q., Wang, Y., Yang, T., Zhang, X., Cheng, J., Sun, J.: You only look one-level feature. In: Proceedings of the IEEE/CVF conference on computer vision and pattern recognition. pp. 13039–13048 (2021)
5. Eykholt, K., Evtimov, I., Fernandes, E., Li, B., Rahmati, A., Xiao, C., Prakash, A., Kohno, T., Song, D.: Robust physical-world attacks on deep learning visual classification. In: Proceedings of the IEEE conference on computer vision and pattern recognition. pp. 1625–1634 (2018)
6. Farin, G.E.: Curves and surfaces for CAGD: a practical guide. Morgan Kaufmann (2002)
7. FLIR Systems: Free flir thermal dataset for algorithm training. <https://oem.flir.com/solutions/automotive/adas-dataset-form/> (2018)
8. Ge, Z., Liu, S., Wang, F., Li, Z., Sun, J.: Yolox: Exceeding yolo series in 2021. arXiv preprint arXiv:2107.08430 (2021)
9. Guesmi, A., Ding, R., Hanif, M.A., Alouani, I., Shafique, M.: Dap: A dynamic adversarial patch for evading person detectors. In: Proceedings of the IEEE/CVF Conference on Computer Vision and Pattern Recognition. pp. 24595–24604 (2024)
10. Ha, Q., Watanabe, K., Karasawa, T., Ushiku, Y., Harada, T.: Mfnet: Towards real-time semantic segmentation for autonomous vehicles with multi-spectral scenes. In: 2017 IEEE/RSJ International Conference on Intelligent Robots and Systems (IROS). pp. 5108–5115. IEEE (2017)
11. Hayes, J.: On visible adversarial perturbations & digital watermarking. In: Proceedings of the IEEE conference on computer vision and pattern recognition workshops. pp. 1597–1604 (2018)
12. He, K., Gkioxari, G., Dollár, P., Girshick, R.: Mask r-cnn. In: Proceedings of the IEEE international conference on computer vision. pp. 2961–2969 (2017)

13. He, K., Zhang, X., Ren, S., Sun, J.: Deep residual learning for image recognition. In: Proceedings of the IEEE conference on computer vision and pattern recognition. pp. 770–778 (2016)
14. Hu, C., Shi, W., Jiang, T., Yao, W., Tian, L., Chen, X., Zhou, J., Li, W.: Adversarial infrared blocks: A multi-view black-box attack to thermal infrared detectors in physical world. *Neural Networks* **175**, 106310 (2024)
15. Hu, C., Shi, W., Yao, W., Jiang, T., Tian, L., Chen, X., Li, W.: Adversarial infrared curves: An attack on infrared pedestrian detectors in the physical world. *Neural networks* **178**, 106459 (2024)
16. Hu, Y.C.T., Kung, B.H., Tan, D.S., Chen, J.C., Hua, K.L., Cheng, W.H.: Naturalistic physical adversarial patch for object detectors. In: Proceedings of the IEEE/CVF international conference on computer vision. pp. 7848–7857 (2021)
17. Hu, Z., Huang, S., Zhu, X., Sun, F., Zhang, B., Hu, X.: Adversarial texture for fooling person detectors in the physical world. In: Proceedings of the IEEE/CVF conference on computer vision and pattern recognition. pp. 13307–13316 (2022)
18. Hwang, S., Park, J., Kim, N., Choi, Y., So Kweon, I.: Multispectral pedestrian detection: Benchmark dataset and baseline. In: Proceedings of the IEEE conference on computer vision and pattern recognition. pp. 1037–1045 (2015)
19. Jia, X., Zhu, C., Li, M., Tang, W., Zhou, W.: Lvip: A visible-infrared paired dataset for low-light vision. In: Proceedings of the IEEE/CVF international conference on computer vision. pp. 3496–3504 (2021)
20. Kennedy, J., Eberhart, R.: Particle swarm optimization. In: Proceedings of ICNN’95-international conference on neural networks. vol. 4, pp. 1942–1948. iee (1995)
21. Lee, C., Song, Y., Son, J.: Data-free universal adversarial perturbation with pseudo-semantic prior. In: Proceedings of the Computer Vision and Pattern Recognition Conference. pp. 13907–13916 (2025)
22. Li, C., Yao, W., Wang, H., Jiang, T.: Adaptive momentum variance for attention-guided sparse adversarial attacks. *Pattern Recognition* **133**, 108979 (2023)
23. Liang, J., Liang, S., Lou, T., Zhang, M., Li, W., Fan, D., Cao, X.: Gradient-reweighted adversarial camouflage for physical object detection evasion. In: Proceedings of the IEEE/CVF International Conference on Computer Vision. pp. 13880–13889 (2025)
24. Lin, T.Y., Goyal, P., Girshick, R., He, K., Dollár, P.: Focal loss for dense object detection. In: Proceedings of the IEEE international conference on computer vision. pp. 2980–2988 (2017)
25. Liu, J., Fan, X., Huang, Z., Wu, G., Liu, R., Zhong, W., Luo, Z.: Target-aware dual adversarial learning and a multi-scenario multi-modality benchmark to fuse infrared and visible for object detection. In: Proceedings of the IEEE/CVF conference on computer vision and pattern recognition. pp. 5802–5811 (2022)
26. Long, J., Yao, W., Jiang, T., Hou, J., Jia, S., Wu, J., Zhang, X., Zheng, X., Ma, C.: Cdupatch: Color-driven universal adversarial patch attack for dual-modal visible-infrared detectors. In: Proceedings of the 33rd ACM International Conference on Multimedia. pp. 1462–1470 (2025)
27. Lou, T., Jia, X., Liang, S., Liang, J., Zhang, M., Xiao, Y., Cao, X.: 3D gaussian splatting driven multi-view robust physical adversarial camouflage generation. In: Proceedings of the IEEE/CVF International Conference on Computer Vision. pp. 28752–28762 (October 2025)
28. Lyu, L., Zhou, J., He, D., Li, Y.: CNCA: Toward customizable and natural generation of adversarial camouflage for vehicle detectors. In: Advances in Neural Information Processing Systems (2024)

29. Madry, A., Makelov, A., Schmidt, L., Tsipras, D., Vladu, A.: Towards deep learning models resistant to adversarial attacks. In: International Conference on Learning Representations (2018)
30. Pang, J., Chen, K., Shi, J., Feng, H., Ouyang, W., Lin, D.: Libra r-cnn: Towards balanced learning for object detection. In: Proceedings of the IEEE/CVF conference on computer vision and pattern recognition. pp. 821–830 (2019)
31. Reddy, K.R., Garg, U., Radhakrishnan, V.B.: Fast feature fool: A data independent approach to universal adversarial perturbations. In: Proceedings of the British Machine Vision Conference (BMVC). BMVA Press (2017). <https://doi.org/10.5244/C.31.30>
32. Redmon, J., Farhadi, A.: Yolov3: An incremental improvement. arXiv preprint arXiv:1804.02767 (2018)
33. Ren, S., He, K., Girshick, R., Sun, J.: Faster r-cnn: Towards real-time object detection with region proposal networks. *Advances in neural information processing systems* **28** (2015)
34. Sakaridis, C., Dai, D., Van Gool, L.: Accd: The adverse conditions dataset with correspondences for semantic driving scene understanding. In: Proceedings of the IEEE/CVF international conference on computer vision. pp. 10765–10775 (2021)
35. Selvaraju, R.R., Cogswell, M., Das, A., Vedantam, R., Parikh, D., Batra, D.: Gradcam: Visual explanations from deep networks via gradient-based localization. In: Proceedings of the IEEE international conference on computer vision. pp. 618–626 (2017)
36. Tan, J., Ji, N., Xie, H., Xiang, X.: Legitimate adversarial patches: Evading human eyes and detection models in the physical world. In: Proceedings of the 29th ACM international conference on multimedia. pp. 5307–5315 (2021)
37. Tao, G., An, S., Cheng, S., Shen, G., Zhang, X.: Hard-label black-box universal adversarial patch attack. In: 32nd USENIX Security Symposium (USENIX Security 23). pp. 697–714 (2023)
38. Teledyne FLIR: Free adas thermal dataset for algorithm training. <https://oem.flir.com/solutions/automotive/adas-dataset-form/> (2022)
39. Thys, S., Van Ranst, W., Goedemé, T.: Fooling automated surveillance cameras: adversarial patches to attack person detection. In: Proceedings of the IEEE/CVF conference on computer vision and pattern recognition workshops. pp. 0–0 (2019)
40. Tiliwalidi, K., Hu, C., Lu, G., Jia, M., Shi, W.: Advgrid: a multi-view black-box attack on infrared pedestrian detectors in the physical world. *Applied Soft Computing* **174**, 112981 (2025)
41. Wei, H., Wang, Z., Jia, X., Zheng, Y., Tang, H., Satoh, S., Wang, Z.: Hotcold block: Fooling thermal infrared detectors with a novel wearable design. In: Proceedings of the AAAI conference on artificial intelligence. vol. 37, pp. 15233–15241 (2023)
42. Wei, X., Yu, J., Huang, Y.: Physically adversarial infrared patches with learnable shapes and locations. In: Proceedings of the IEEE/CVF conference on computer vision and pattern recognition. pp. 12334–12342 (2023)
43. Wu, Z., Lim, S.N., Davis, L.S., Goldstein, T.: Making an invisibility cloak: Real world adversarial attacks on object detectors. In: European Conference on Computer Vision. pp. 1–17. Springer (2020)
44. Zhang, R., Isola, P., Efros, A.A., Shechtman, E., Wang, O.: The unreasonable effectiveness of deep features as a perceptual metric. In: Proceedings of the IEEE conference on computer vision and pattern recognition. pp. 586–595 (2018)
45. Zhou, J., Lyu, L., He, D., Li, Y.: RAUCA: A novel physical adversarial attack on vehicle detectors via robust and accurate camouflage generation. In: Proceedings

- of the 41st International Conference on Machine Learning. Proceedings of Machine Learning Research, vol. 235, pp. 62076–62087. PMLR (2024)
46. Zhu, X., Hu, Z., Huang, S., Li, J., Hu, X.: Infrared invisible clothing: Hiding from infrared detectors at multiple angles in real world. In: Proceedings of the IEEE/CVF Conference on Computer Vision and Pattern Recognition. pp. 13317–13326 (2022)
 47. Zhu, X., Hu, Z., Huang, S., Li, J., Hu, X., Wang, Z.: Hiding from infrared detectors in real world with adversarial clothes: X. zhu et al. *Applied Intelligence* **53**, 29537–29555 (2023)
 48. Zhu, X., Li, X., Li, J., Wang, Z., Hu, X.: Fooling thermal infrared pedestrian detectors in real world using small bulbs. In: Proceedings of the AAAI conference on artificial intelligence. vol. 35, pp. 3616–3624 (2021)
 49. Zhu, X., Liu, Y., Hu, Z., Li, J., Hu, X.: Infrared adversarial car stickers. In: Proceedings of the IEEE/CVF Conference on Computer Vision and Pattern Recognition. pp. 24284–24293 (2024). <https://doi.org/10.1109/CVPR52733.2024.02292>
 50. Zhu, X., Su, W., Lu, L., Li, B., Wang, X., Dai, J.: Deformable detr: Deformable transformers for end-to-end object detection. In: International Conference on Learning Representations (2021)